Pergamon

Int. J. Solids Structures Vol. 32, No. 8/9, pp. 1211–1230, 1995

0020–7683/95 $9.50 + .00

0020–7683(94)00144–8

THREE-DIMENSIONAL STABILITY ANALYSIS OF LAMINATED ANISOTROPIC CIRCULAR CYLINDERS

S. B. DONG and P. ETITUM†
Civil and Environmental Engineering Department, University of California at Los Angeles, Los Angeles, CA 90024, U.S.A.

(*Received* 11 *January* 1994; *in revised form* 22 *June* 1994)

Abstract—Linear bifurcation stability of laminated anisotropic circular cylinders is investigated on the basis of three-dimensional elasticity using Biot's incremental deformation theory. A finite element code employing radial discretization is formulated for the calculations. By this approach, the laminate's thickness profile may be composed of an arbitrary number of bonded elastic anisotropic layers, each of which may have its own mechanical properties, thickness and initial stress state. Using a solution that is periodic axially and circumferentially in the variationally derived equilibrium equations yields an algebraic eigenvalue problem, where the critical (lowest) eigenvalue is sought. It represents the ratio of the buckling stress state to initial stress state and its associated eigenvector contains the radial distribution of the displacements. A parametric study on a series of regular symmetric and antisymmetric cross-ply and angle-ply laminated composite cylinders under axial compression and torsion was conducted, where the data can be used to assess the accuracy and range of validity of stability predictions based on shell theories. An example of the axial compression of a thick-walled laminated composite cylinder is presented to illustrate an instability phenomenon where internal and surface deformations are present.

INTRODUCTION

A circular cylindrical tube fabricated of laminated composite material(s) represents a structural shape enjoying wide applications in many industries. One concern in the design of circular cylinders, particularly when they are thin-walled, is the loss of structural stability. This paper deals with a linear elastic stability analysis of laminated composite circular cylinders using Biot's incremental deformation theory (1965). The proposed technique, based on finite elements, can be applied to arbitrary laminate profiles of anisotropic materials. Biot's theory rests on linear three-dimensional elasticity and uses linearized deformational measures about a self-equilibrated initially stressed state to describe the subsequent response due to incremental loading. Applying Biot's theory to linear stability problems leads to results pertaining to bifurcation buckling. By a three-dimensional formulation, it is also possible to predict internal buckling, an instability mode where deformations occur primarily within the body. Delamination may be a consequence of internal buckling, to which cylinders with low radius/thickness ratios and low transverse normal stiffness are more susceptible.

The semi-analytical finite element technique presented herein is based on the modeling of the radial dependence of the behavior in the cylinder by polynomials in the discretized cylindrical laminae. Each lamina is capable of representing distinct local elastic, anisotropic properties as well as the stress components comprising the arbitrary self-equilibrated initial state. Quadratic polynomials are used in the radial direction, with nodal degrees of freedom at the lamina's two bounding surfaces and its mid-point. At these nodes, the axial and circumferential dependencies are left unspecified at the outset. This radial discretization procedure was used by Bradford and Dong (1978) for studying vibrations of initially stressed laminated orthotropic (or general cross-ply) cylinders, and the present finite element code extends the capability to treat completely anisotropic materials. Also, the present code is based on isoparametric methodology and numerical integration, instead of the

†Currently a Director of Vibro(Thai) Ltd., Bangkok, Thailand.

algebraically more cumbersome exact integration of Bradford and Dong (1978). The governing partial differential equations of equilibrium are obtained by varying the total incremental potential energy including contributions due to initial stress. They are in terms of the nodal displacements as functions of the axial and circumferential coordinate variables. Upon invoking the axial and circumferential dependencies in the solution form for the buckled shape, the set of governing equations is transformed into an algebraic eigenvalue problem. The lowest eigenvalue represents the ratio of the critical (i.e. bifurcation) stress level to the reference or self-equilibrated initial stress state. The corresponding eigenvector depicts the radial pattern of displacements of the buckled shape.

A parametric study is presented for axial compression and torsion loading conditions of regular cross-ply and angle-ply cylinders. The parameters of interest include the numbers of plies in the laminate profiles, cross-ply and angle-ply layups, and thickness/radius ratios simulating both thin and thick shell geometries. The numerical results are summarized in graphical form, showing the lowest bifurcation load as functions of the length/radius ratio and circumferential mode numbers. One case of a laminated composite thick-walled cylinder under axial compression is considered to show some aspects of internal buckling.

In connection with the present method of stability analysis, attention is called to Kardomateas (1993a, b) who studied the linear buckling of homogeneous, orthotropic circular cylinders on the basis of three-dimensional elasticity. His governing stability equations are essentially identical to those of Biot's theory, although the points of departure in the derivations differ somewhat. Kardomateas investigated linear bifurcation buckling for axial compression and pressurization loading conditions analytically, the latter under plane strain deformation. While his method can be extended to treat layered cylinders, the potentially inordinate algebraic details will undoubtedly be an inhibiting factor limiting the extent of numerical results. The present finite element method, while incapable of tracking behavioral inter-relations analytically, does permit completely arbitrary laminate profiles of distinct anisotropic materials to be treated in a straightforward way.

As three-dimensional elasticity data may be regarded as exact for all radius/thickness ratios, they can serve as the basis for comparing the accuracy and range of application of classical and refined shell theories. In contrast to homogeneous, isotropic materials, the classical shell theory for laminated fiber composites suffers from a reduced range of application because the low transverse shear and normal stiffnesses cause the behavior to depart from the underlying kinematic hypotheses more readily. The need to account for these two effects has prompted development of various refined theories, where the behavioral differences between them are rooted in the respective constitutive relations. In arguing the viability of these theories, most authors point to the differences between their results with those of classical theory and/or a lower order refined theory. A more convincing tactic is by comparison with three-dimensional elasticity data. The present solution technique generates such data with ease. In a companion paper by Etitum and Dong (1994), a comprehensive parametric study is given to shed light on the accuracy and the range of application of classical and first-order shear deformation theories in buckling analyses.

Some limitations regarding the present analysis need to be mentioned.

(1) That initial imperfections in cylindrical shells play a very dominant role in limiting the maximum load carrying capacity has not escaped the attention of the authors. The voluminous literature cited by Hutchinson and Koiter (1970) primarily on homogeneous, isotropic cylinders and by Simitses (1986) on laminated composite cylinders certainly underscores this point. But, imperfection sensitivity is not taken up herein, with the plea that issues related to the parameters governing bifurcation instability are sufficient to fully occupy a meaningful discussion.
(2) Geometrically nonlinear prebuckled deformations are ignored. Only linear bifurcation is treated based on a given initial stress state whose load path arriving at this state is deemed to be of no consequence to the buckling results. Although it is possible to account for a geometrically nonlinear prebuckled state, the computational effort would be greater and beyond the current scope.

(3) The initial stress states used in the buckling analysis herein are simple two-dimensional (generalized plane stress) states, reminiscent of the stress resultants assumed in shell and plate theory calculations. This approach suits the purpose of this paper for providing equivalent comparison data. However, the method accommodates a general three-dimensional stress state, which may be, for example, the results of extension/torsion of a laminated circular cylinder (i.e. the Saint-Venant problem) and of internal and external pressurization. At present, this capability is not readily available. Nevertheless, the need for an accurate three-dimensional stress state is relevant and must be emphasized, especially in internal buckling phenomenon, whose behavior is intricately three-dimensional and complex.

These caveats are important issues and deserve appropriate attention in order for a full understanding of the stability behavior of laminated anisotropic cylinders. The method herein represents a stepping stone toward this goal.

BASIC EQUATIONS

Let cylindrical coordinates $(r, \theta, x\dagger)$ be adopted. The mechanical variables of the problem are the three displacements $u_i(r, \theta, x)$, six stress and strain components $\sigma_{ij}(r, \theta, x)$ and $\varepsilon_{ij}(r, \theta, x)$, and three infinitesimal rigid body rotations $\omega_i(r, \theta, x)$. These variables describe an incremental deformed state with respect to a reference equilibrium state whose stress components are denoted by $S_{ij}(r, \theta, x)$. The components of these variables are listed in the following arrays:

$$\mathbf{u} = [u_r \quad u_\theta \quad u_x]^T \tag{1}$$

$$\boldsymbol{\sigma} = [\sigma_{rr} \quad \sigma_{\theta\theta} \quad \sigma_{xx} \quad \sigma_{\theta x} \quad \sigma_{rx} \quad \sigma_{r\theta}]^T \tag{2}$$

$$\boldsymbol{\varepsilon} = [\varepsilon_{rr} \quad \varepsilon_{\theta\theta} \quad \varepsilon_{xx} \quad \gamma_{\theta x} \quad \gamma_{rx} \quad \gamma_{r\theta}]^T \tag{3}$$

$$\boldsymbol{\varepsilon}_\omega = [\varepsilon_{rr} \quad \varepsilon_{\theta\theta} \quad \varepsilon_{xx} \quad \varepsilon_{\theta x} \quad \varepsilon_{rx} \quad \varepsilon_{r\theta} \quad \omega_r \quad \omega_\theta \quad \omega_x]^T \tag{4}$$

$$\boldsymbol{\sigma}_S = [S_{rr} \quad S_{\theta\theta} \quad S_{xx} \quad S_{\theta x} \quad S_{rx} \quad S_{r\theta}]^T. \tag{5}$$

Observe that $\boldsymbol{\varepsilon}_\omega$ contains both rigid body rotations ω_i, and tensorial strain components $\varepsilon_{ij} = \gamma_{ij}/2$ $(i \neq j)$. This particular form will facilitate the finite element development. Note that the loading history leading to the reference equilibrium state is assumed to have no bearing on the subsequent incremental elastic deformation. Only the magnitude of this stress state plays a role.

The strain–displacement relations for the components in $\boldsymbol{\varepsilon}$ and $\boldsymbol{\varepsilon}_\omega$ are written in terms of three differential operators, each involving differentiation of an independent spatial coordinate:

$$\boldsymbol{\varepsilon} = (L_{r1} + L_{\theta 1} + L_{x1})\mathbf{u}, \quad \boldsymbol{\varepsilon}_\omega = (L_{r2} + L_{\theta 2} + L_{x2})\mathbf{u} \tag{6}$$

where the operators $(L_{r1}, L_{\theta 1}, L_{x1})$ and $(L_{r2}, L_{\theta 2}, L_{x2})$ are given in the Appendix.

The incremental stress–strain relation is given by

$$\boldsymbol{\sigma} = \mathbf{C}\boldsymbol{\varepsilon} \tag{7}$$

where $\mathbf{C}$ is a (6×6) matrix of cylindrically anisotropic elastic moduli. In the variational principle to be stated, the six initial stress components S_{ij} participate in a (9×9) matrix $\mathbf{S}$ of the form

†The variable x is used for the axial coordinate rather than z for circular cylindrical coordinates to be in keeping with cylindrical shell theory notation.

$$\mathbf{S} = \begin{vmatrix} \cdot & \cdot & \cdot & \cdot & \cdot & \cdot & \cdot & -S_{rx} & S_{r\theta} \\ & \cdot & \cdot & \cdot & \cdot & \cdot & S_{\theta x} & \cdot & -S_{r\theta} \\ & & \cdot & \cdot & \cdot & \cdot & -S_{\theta x} & S_{rx} & \cdot \\ & & & \cdot & \cdot & \cdot & S_{xx}-S_{\theta\theta} & S_{r\theta} & -S_{rx} \\ & & & & \cdot & \cdot & -S_{r\theta} & S_{rr}-S_{xx} & S_{\theta x} \\ & & & & & \cdot & S_{rx} & -S_{\theta x} & S_{\theta\theta}-S_{rr} \\ & & & & & & S_{\theta\theta}+S_{xx} & -S_{r\theta} & -S_{rx} \\ & \text{sym} & & & & & & S_{rr}+S_{xx} & -S_{\theta x} \\ & & & & & & & & S_{rr}+S_{\theta\theta} \end{vmatrix} . \tag{8}$$

The theorem of minimum potential energy in the form

$$\delta(\Delta V_1 + \Delta V_2 + \Delta W_e) = 0 \tag{9}$$

provides the displacement equations of equilibrium and boundary conditions where $\Delta V_1, \Delta V_2$ and ΔV_e are the incremental energies of strain, initial stress and applied incremental tractions given by

$$\Delta V_1 = \frac{1}{2}\iiint_B \boldsymbol{\varepsilon}^T \mathbf{C}\boldsymbol{\varepsilon} r \, dr \, d\theta \, dz \tag{10}$$

$$\Delta V_2 = \frac{1}{2}\iiint_B \boldsymbol{\varepsilon}_\omega^T \mathbf{S}\boldsymbol{\varepsilon}_\omega r \, dr \, d\theta \, dz \tag{11}$$

$$\Delta W_e = -\iint_S \mathbf{u}_S^T \Delta\mathbf{f} \, dS \tag{12}$$

where $\Delta\mathbf{f}$ is the array of surface traction components and $\mathbf{u}_s$ denotes the displacement components along directions corresponding to the applied tractions.

SEMI-ANALYTICAL FINITE ELEMENTS

In this version of the finite element method, the radial profile of the cylinder is discretized into cylindrical laminae. Within each lamina, the radial dependence of the displacement field is modeled by quadratic polynomials using three nodes, two at the bounding surfaces and one at the mid-point of the lamina (see Fig. 1). These nodal degrees of freedom are undetermined functions of (θ, x). The interpolation field within a lamina is given by

$$\begin{aligned} u_r(r,\theta,x) &= \mathbf{n}\mathbf{u}_r = [n_1(\xi)n_2(\xi)n_3(\xi)]\mathbf{u}_r(\theta,x) \\ u_\theta(r,\theta,x) &= \mathbf{n}\mathbf{u}_\theta = [n_1(\xi)n_2(\xi)n_3(\xi)]\mathbf{u}_\theta(\theta,x) \\ u_x(r,\theta,x) &= \mathbf{n}\mathbf{u}_x = [n_1(\xi)n_2(\xi)n_3(\xi)]\mathbf{u}_x(\theta,x) \end{aligned} \tag{13}$$

where the interpolation functions n_is in local coordinate ξ are

$$n_1 = \tfrac{1}{2}\xi(\xi-1), \quad n_2 = 1-\xi^2, \quad n_3 = \tfrac{1}{2}\xi(\xi+1), \quad (-1 \leqslant \xi \leqslant +1), \tag{14}$$

and the arrays $\mathbf{u}_r$, $\mathbf{u}_\theta$, $\mathbf{u}_x$ contain the respective nodal displacement components. Isoparametric finite element methodology is followed using numerical integration, the details of which are standard and need no elaboration [see, for example, Zienkiewicz (1978)]. This

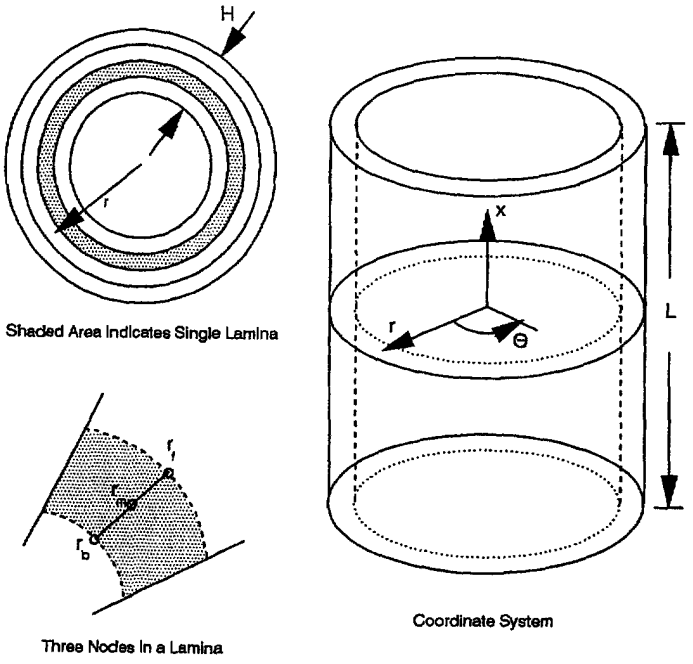

Note: 0° Ply Angle is parallel to the x-axis.

Fig. 1. Nodes of laminae.

separation of the dependent variables with one part of the decomposition explicitly stated is an approach situated intermediate of an exact solution and the Ritz/Galerkin methods. This general approach is attributed to Kantorovich and Krylov (1958) and is known as the semi-analytical technique in finite element nomenclature.

To facilitate the discussion, assemble the element displacement interpolations into one over the total thickness of the cylinder:

$$\begin{bmatrix} u_r(r,\theta,x) \\ u_\theta(r,\theta,x) \\ u_x(r,\theta,x) \end{bmatrix} = \begin{bmatrix} N(r) & \cdot & \cdot \\ \cdot & N(r) & \cdot \\ \cdot & \cdot & N(r) \end{bmatrix} \begin{bmatrix} \{U_r(\theta,x)\} \\ \{U_\theta(\theta,x)\} \\ \{U_x(\theta,x)\} \end{bmatrix} \tag{15}$$

or in abbreviated matrix form

$$\mathbf{u} = \mathbf{NU}, \tag{15a}$$

where $N(r)$ contain the assembled finite element interpolations and $\mathbf{U}(\theta, x)$ represents the ordered set of nodal displacements over the entire thickness profile. Substitution of eqn (15) into eqn (6) gives

$$\boldsymbol{\varepsilon} = L_{r1}(\mathbf{NU}) + L_{\theta 1}(\mathbf{NU}) + L_{x1}(\mathbf{NU}) = \mathbf{B}_{r1}\mathbf{U} + \mathbf{B}_{\theta 1}\mathbf{U}_{,\theta} + \mathbf{B}_{x1}\mathbf{U}_{,x} \tag{16}$$

$$\boldsymbol{\varepsilon}_\omega = L_{r2}(\mathbf{NU}) + L_{\theta 2}(\mathbf{NU}) + L_{x2}(\mathbf{NU}) = \mathbf{B}_{r2}\mathbf{U} + \mathbf{B}_{\theta 2}\mathbf{U}_{,\theta} + \mathbf{B}_{x2}\mathbf{U}_{,x} \tag{17}$$

where strain–transformation matrices $(\mathbf{B}_{r1}, \mathbf{B}_{\theta 1}, \mathbf{B}_{x1})$ and $(\mathbf{B}_{r2}, \mathbf{B}_{\theta 2}, \mathbf{B}_{x2})$ are defined in the Appendix. Substituting eqns (15)–(17) into eqns (10)–(12) gives

$$\Delta V_1 = \frac{1}{2}\iiint_B (\mathbf{U}^{\mathrm{T}}\mathbf{B}_{r1}^{\mathrm{T}}\mathbf{C}\mathbf{B}_{r1}\mathbf{U} + \mathbf{U}^{\mathrm{T}}\mathbf{B}_{r1}^{\mathrm{T}}\mathbf{C}\mathbf{B}_{\theta 1}\mathbf{U}_{,\theta} + \mathbf{U}^{\mathrm{T}}\mathbf{B}_{r1}^{\mathrm{T}}\mathbf{C}\mathbf{B}_{x1}\mathbf{U}_{,x}$$
$$+ \mathbf{U}_{,\theta}^{\mathrm{T}}\mathbf{B}_{\theta 1}^{\mathrm{T}}\mathbf{C}\mathbf{B}_{r1}\mathbf{U} + \mathbf{U}_{,\theta}^{\mathrm{T}}\mathbf{B}_{\theta 1}^{\mathrm{T}}\mathbf{C}\mathbf{B}_{\theta 1}\mathbf{U}_{,\theta} + \mathbf{U}_{,\theta}^{\mathrm{T}}\mathbf{B}_{\theta 1}^{\mathrm{T}}\mathbf{C}\mathbf{B}_{x1}\mathbf{U}_{,x}$$
$$+ \mathbf{U}_{,x}^{\mathrm{T}}\mathbf{B}_{x1}^{\mathrm{T}}\mathbf{C}\mathbf{B}_{r1}\mathbf{U} + \mathbf{U}_{,x}^{\mathrm{T}}\mathbf{B}_{x1}^{\mathrm{T}}\mathbf{C}\mathbf{B}_{\theta 1}\mathbf{U}_{,\theta} + \mathbf{U}_{,x}^{\mathrm{T}}\mathbf{B}_{x1}^{\mathrm{T}}\mathbf{C}\mathbf{B}_{x1}\mathbf{U}_{,x})\, r\,\mathrm{d}r\,\mathrm{d}\theta\,\mathrm{d}x \tag{18}$$

$$\Delta V_2 = \frac{1}{2}\iiint_B (\mathbf{U}^{\mathrm{T}}\mathbf{B}_{r2}^{\mathrm{T}}\mathbf{S}\mathbf{B}_{r2}\mathbf{U} + \mathbf{U}^{\mathrm{T}}\mathbf{B}_{r2}^{\mathrm{T}}\mathbf{S}\mathbf{B}_{\theta 2}\mathbf{U}_{,\theta} + \mathbf{U}^{\mathrm{T}}\mathbf{B}_{r2}^{\mathrm{T}}\mathbf{S}\mathbf{B}_{x2}\mathbf{U}_{,x}$$
$$+ \mathbf{U}_{,\theta}^{\mathrm{T}}\mathbf{B}_{\theta 2}^{\mathrm{T}}\mathbf{S}\mathbf{B}_{r2}\mathbf{U} + \mathbf{U}_{,\theta}^{\mathrm{T}}\mathbf{B}_{\theta 2}^{\mathrm{T}}\mathbf{S}\mathbf{B}_{\theta 2}\mathbf{U}_{,\theta} + \mathbf{U}_{\theta}^{\mathrm{T}}\mathbf{B}_{\theta 2}^{\mathrm{T}}\mathbf{S}\mathbf{B}_{x2}\mathbf{U}_{,x}$$
$$+ \mathbf{U}_{,x}^{\mathrm{T}}\mathbf{B}_{x2}^{\mathrm{T}}\mathbf{S}\mathbf{B}_{r2}\mathbf{U} + \mathbf{U}_{,x}^{\mathrm{T}}\mathbf{B}_{x2}^{\mathrm{T}}\mathbf{S}\mathbf{B}_{\theta 2}\mathbf{U}_{,\theta} + \mathbf{U}_{,x}^{\mathrm{T}}\mathbf{B}_{x2}^{\mathrm{T}}\mathbf{S}\mathbf{B}_{x2}\mathbf{U}_{,x})\, r\,\mathrm{d}r\,\mathrm{d}\theta\,\mathrm{d}x \tag{19}$$

$$\Delta W_{\mathrm{e}} = \iint_S \mathbf{U}^{\mathrm{T}}\mathbf{N}_s\Delta\mathbf{f}\, r\,\mathrm{d}s\,\mathrm{d}\theta. \tag{20}$$

Carrying out the variation indicated by eqn (9) gives

$$\mathbf{K}_1\mathbf{U} + \mathbf{K}_2\mathbf{U}_{,\theta} + \mathbf{K}_3\mathbf{U}_{,x} - \mathbf{K}_4\mathbf{U}_{,\theta\theta} - \mathbf{K}_5\mathbf{U}_{,\theta x} - \mathbf{K}_6\mathbf{U}_{,xx}$$
$$+ \mathbf{K}_{g1}\mathbf{U} + \mathbf{K}_{g2}\mathbf{U}_{,\theta} + \mathbf{K}_{g3}\mathbf{U}_{,x} - \mathbf{K}_{g4}\mathbf{U}_{,\theta\theta} - \mathbf{K}_{g5}\mathbf{U}_{,\theta x} - \mathbf{K}_{g6}\mathbf{U}_{,xx} = \Delta\mathbf{F}(\theta, x) \tag{21}$$

where

$$\mathbf{K}_1 = \int_r \mathbf{B}_{r1}^{\mathrm{T}}\mathbf{C}\mathbf{B}_{r1}\, r\,\mathrm{d}r, \quad \mathbf{K}_2 = \int_r (\mathbf{B}_{r1}^{\mathrm{T}}\mathbf{C}\mathbf{B}_{\theta 1} - \mathbf{B}_{\theta 1}^{\mathrm{T}}\mathbf{C}\mathbf{B}_{r1})\, r\,\mathrm{d}r$$
$$\mathbf{K}_4 = \int_r \mathbf{B}_{\theta 1}^{\mathrm{T}}\mathbf{C}\mathbf{B}_{\theta 1}\, r\,\mathrm{d}r, \quad \mathbf{K}_3 = \int_r (\mathbf{B}_{r1}^{\mathrm{T}}\mathbf{C}\mathbf{B}_{x1} - \mathbf{B}_{x1}^{\mathrm{T}}\mathbf{C}\mathbf{B}_{r1})\, r\,\mathrm{d}r \tag{22}$$

$$\mathbf{K}_6 = \int_r \mathbf{B}_{x1}^{\mathrm{T}}\mathbf{C}\mathbf{B}_{x1}\, r\,\mathrm{d}r, \quad \mathbf{K}_5 = \int_r (\mathbf{B}_{\theta 1}^{\mathrm{T}}\mathbf{C}\mathbf{B}_{x1} + \mathbf{B}_{x1}^{\mathrm{T}}\mathbf{C}\mathbf{B}_{\theta 1})\, r\,\mathrm{d}r$$
$$\mathbf{K}_{g1} = \int_r \mathbf{B}_{r2}^{\mathrm{T}}\mathbf{S}\mathbf{B}_{r2}\, r\,\mathrm{d}r, \quad \mathbf{K}_{g2} = \int_r (\mathbf{B}_{r2}^{\mathrm{T}}\mathbf{S}\mathbf{B}_{\theta 2} - \mathbf{B}_{\theta 2}^{\mathrm{T}}\mathbf{S}\mathbf{B}_{r2})\, r\,\mathrm{d}r$$
$$\mathbf{K}_{g4} = \int_r \mathbf{B}_{\theta 2}^{\mathrm{T}}\mathbf{S}\mathbf{B}_{\theta 2}\, r\,\mathrm{d}r, \quad \mathbf{K}_{g3} = \int_r (\mathbf{B}_{r2}^{\mathrm{T}}\mathbf{S}\mathbf{B}_{x2} - \mathbf{B}_{x2}^{\mathrm{T}}\mathbf{S}\mathbf{B}_{r2})\, r\,\mathrm{d}r$$
$$\mathbf{K}_{g6} = \int_r \mathbf{B}_{x2}^{\mathrm{T}}\mathbf{S}\mathbf{B}_{x2}\, r\,\mathrm{d}r, \quad \mathbf{K}_{g5} = \int_r (\mathbf{B}_{\theta 2}^{\mathrm{T}}\mathbf{S}\mathbf{B}_{x2} + \mathbf{B}_{x2}^{\mathrm{T}}\mathbf{S}\mathbf{B}_{\theta 2})\, r\,\mathrm{d}r \tag{23}$$

$$\Delta\mathbf{F} = \mathbf{N}_s\Delta\mathbf{f}. \tag{24}$$

Equation (21) is the governing displacement equation of equilibrium that can be used to determine the incremental deformation due to the incremental applied load $\Delta\mathbf{F}$. Note that $\mathbf{K}_1, \mathbf{K}_4, \mathbf{K}_5, \mathbf{K}_6, \mathbf{K}_{g1}, \mathbf{K}_{g4}, \mathbf{K}_{g5}, \mathbf{K}_{g6}$ are symmetric while $\mathbf{K}_2, \mathbf{K}_3, \mathbf{K}_{g2}, \mathbf{K}_{g3}$ are antisymmetric.

LINEAR STABILITY ANALYSIS

For a linear elastic stability problem, suppress $\Delta\mathbf{F}$ in eqn (21). Introduce the parameter Λ for denoting the ratio of the critical initial stress state to the given initial stress state, i.e.

$$\Lambda = \sigma_{\text{init(crit)}}/\sigma_{\text{init}}, \tag{25}$$

and take the analytical form of the buckled shape as

$$\mathbf{U}(\theta, x) = \mathbf{U}_o\, e^{i(kx-n\theta)} \tag{26}$$

where (k, n) are axial and circumferential wave numbers and $\mathbf{U}_o$ is the array of nodal displacements over the thickness. This solution form assumes periodic boundary conditions along the generator of the cylinder with repeating fields over a buckled wave length L, where $L = 2\pi/k$. More will be said on the nature of the boundary conditions inherent in representation (26) in the next section. Substituting solution form (26) in the homogeneous form of eqn (21) and using the parameter Λ lead to the following algebraic eigensystem with complex matrices

$$(\mathbf{K}_R + i\mathbf{K}_I)\mathbf{U}_o + \Lambda(\mathbf{K}_{gR} + i\mathbf{K}_{gI})\mathbf{U}_o = 0 \tag{27}$$

where

$$\mathbf{K}_R = \mathbf{K}_1 + n^2\mathbf{K}_4 + nk\mathbf{K}_5 + k^2\mathbf{K}_6, \qquad \mathbf{K}_I = n\mathbf{K}_2 + k\mathbf{K}_3 \tag{28}$$

$$\mathbf{K}_{gR} = \mathbf{K}_{g1} + n^2\mathbf{K}_{g4} + nk\mathbf{K}_{g5} + k^2\mathbf{K}_{g6}, \quad \mathbf{K}_{gI} = n\mathbf{K}_{g2} + k\mathbf{K}_{g3}. \tag{29}$$

In eqn (27), note that the complex form is Hermitian by virtue of the symmetric real and antisymmetric imaginary components as shown in eqns (28) and (29). Therefore, only real eigenvalues are contained in the system. Eigenvalue problem (27) can be rendered purely real by doubling its size as follows:

$$\begin{bmatrix} \mathbf{K}_R & -\mathbf{K}_I \\ \mathbf{K}_I & \mathbf{K}_R \end{bmatrix} \begin{Bmatrix} \mathbf{U}_o \\ -i\mathbf{U}_o \end{Bmatrix} + \Lambda \begin{bmatrix} \mathbf{K}_{gR} & -\mathbf{K}_{gI} \\ \mathbf{K}_{gI} & \mathbf{K}_{gR} \end{bmatrix} \begin{Bmatrix} \mathbf{U}_o \\ -i\mathbf{U}_o \end{Bmatrix} = 0. \tag{30}$$

The symmetry of all matrices is easily observed in eqn (30). Solution of eqn (30) provides the critical value of Λ representing the bifurcation buckling load ratio. Its associated eigenvector depicts the radial displacement of the buckled shape. Only the lowest eigenvalue is of physical importance and herein it is extracted by subspace iteration using a subset of displacements based on applied loads as the starting vectors [see Dong *et al.* (1972); Dong and Wolf (1970)].

NATURE OF PERIODIC BOUNDARY CONDITIONS

To understand the periodic nature of solution form (26), consider $\mathbf{U}_o$ as complex, i.e. $\mathbf{U}_o = \mathbf{U}_{oR} + i\mathbf{U}_{oI}$ and expand the exponential function into trigonometric functions as

$$\mathbf{U}(x, \theta) = \mathbf{U}_{oR}\cos(kx+n\theta) - \mathbf{U}_{oI}\sin(kx+n\theta) + i\,(\mathbf{U}_{oR}\sin(kx+n\theta) + \mathbf{U}_{oI}\cos(kx+n\theta)). \tag{31}$$

In this form, the periodic roles of both the real and imaginary parts of $\mathbf{U}_o$ are clearly seen.

For a generally cross-ply cylinder, periodic solutions portray simply supported conditions (i.e. mixed conditions). Its manifestation in eigensystem (30) takes the form of two identical, decoupled subsets of matrices with repeated eigendata. Each displacement eigenvector in the repeated pair bears a phase difference of $\pi/2$ with the other.

For a completely anisotropic cylinder, there are also repeated eigendata pairs. However, there is no meaningful analogue to simple supports as the displacement eigenvector is complex. The only description of periodicity is that the solution repeats itself over intervals of length L.

Table 1.

Laminate profile		Figure numbers for Axial compression	Figure numbers for Torsion
Symmetric cross-ply	[0,90,0,...,90,0]	2	8
Antisymmetric cross-ply	[0,90,....,0,90]	3(a)	9(a)
Antisymmetric cross-ply	[90,0,....,90,0]	3(b)	9(b)
Symmetric angle-ply	[+45,−45,...,−45,+45]	4(a)	10(a)
Antisymmetric angle-ply	[+45,−45,...,+45,−45]	4(b)	10(b)
Symmetric angle-ply	[+30,−30,...,−30,+30]	5(a)	11(a)
Antisymmetric angle-ply	[+30,−30,..,+30,−30]	5(b)	11(b)

To treat general boundary conditions using Biot's theory, a two-dimensional (axisymmetric) finite element code is needed where interpolations occur over a meridional plane. Then, general boundary conditions can be enforced at the ends of the finite length cylinder. Such a code has been developed [see Pham (1989)], but no recourse is made to it since the required computational labor is one order of magnitude more intensive. Since comparisons of the present results with classical and first-order shear deformation theories in a companion paper by Etitum and Dong (1994) are under commensurable conditions, solution form (26) should not be overly restrictive in studying a wide range of parameters that influence bifurcation buckling.

PARAMETRIC STUDY ON CYLINDRICAL SHELLS

In this section, the results of a parametric study of cylindrical shell stability under axial compression and torsion are presented. Three regular symmetric and four regular antisymmetric types of laminate profiles were considered and they are summarized in Table 1. A regular laminate refers to a layup where all plies have the same thickness and same mechanical properties, and symmetric and antisymmetric profiles pertain to the total number of plies being odd and even, respectively. In this study, only one material system was considered, that being a transversely isotropic material with properties

$$\frac{E_L}{E_T} = 25, \quad \frac{G_{LT}}{E_T} = 0.5, \quad \frac{G_{TT}}{E_T} = 0.4, \quad \nu_{LT} = 0.25, \quad \nu_{TT} = 0.25. \tag{32}$$

In this study, the number of plies for symmetric laminates ranged from three to nine, and that for antisymmetric laminates from two to eight. The total laminate thickness is denoted by H.

Two geometric parameters were considered. One is the buckled wave length in the form of the ratio (L/a), where a is the mean radius of the cylinder. This parameter ranged from 0.1 to 250. The other is the thickness ratio (H/a) and two cases were considered; $H/a = 0.01$ representing a thin shell geometry and $H/a = 0.1$ for a thick shell geometry. All stability results are presented in graphical form of the critical (lowest) dimensionless stress versus L/a. The circumferential mode number n associated with the critical stress is indicated.

To refresh our understanding of buckling for different laminate profiles, it is useful to recall certain behavioral features of regular symmetric and antisymmetric laminates as predicted by lamination theory.† For symmetric laminates, the middle surface is a structural symmetry plane so that all B_{ij}s are absent. Consequently, there is no extensional/bending coupling. For regular antisymmetric laminates, extensional/bending coupling occurs in the following ways. For cross-ply laminates, only coefficients B_{11} and B_{22} exist with $B_{11} = -B_{22}$. For angle-ply laminates, only coefficients B_{16} and B_{26} are present. These coefficients go to zero with increasing numbers of pairs of plies. Extensional/bending coupling generally

†The reader may wish to refer to a text devoted to lamination theory, such as Tsai and Hahn (1980).

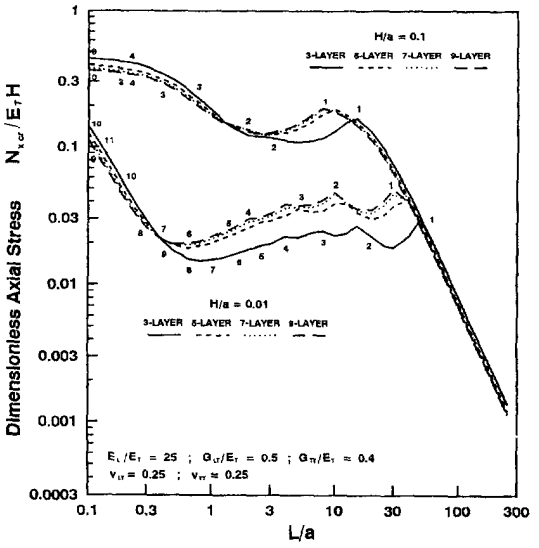

Fig. 2. Axial buckling of regular symmetric cross-ply cylinders.

degrades the flexural stiffness, manifesting in lower buckling loads if substantial bending is involved. Thus, the lowest buckling loads occur in two layer profiles because the B_{ij}s are the largest in magnitude. This pattern should be seen in the present results.

Axial compression

The axial strain is assumed to be uniform over the cylinder's cross-section under axial compression and the axial stress is proportional to the axial stiffness. Hence, for angle-ply laminates, the stress distribution is uniform over the cross-section. However, for cross-ply laminates composed of materials with properties given by eqn (32), $\sigma_{xx}^{90^\circ} = 25\sigma_{xx}^{0}$.

The dimensionless buckling stress for axial compression is given by $N_{x\,cr}/E_T H$, where N_x denotes the axial force per unit circumferential distance around the mid-surface of the cylinder. Plots of the critical (lowest) dimensionless axial stress as a function of L/a for the seven laminate cases are given in Figs 2–5 (refer to Table 1 for description of the laminate profiles). Some observations of these results are presented below.

For the symmetric cross-ply laminates, even though there is no extensional/bending coupling, the data in Fig. 2 for the thin shell geometry show a significantly lower critical stress for the three layer profiles in comparison to the other layups over a significant range of L/a. This pattern shows a dramatic contrast with data for symmetric ($\pm 45^\circ$) and ($\pm 30^\circ$) laminates in Figs 4(a) and 5(a), where the difference between the three layer profile and the others is much less.

In all antisymmetric laminates, the characteristic of the two layer profile being tied to a significantly lower critical stress in comparison to the other layups is seen repeatedly, i.e. in the ($0^\circ/90^\circ$), ($90^\circ/0^\circ$), ($\pm 45^\circ$) and ($\pm 30^\circ$) data in Figs 3(a,b), 4(b), and 5(b), respectively. There appears to be little difference in the buckling data between the ($0^\circ/90^\circ$) and ($90^\circ/0^\circ$) cross-ply laminates as shown in Figs 3(a) and 3(b).

Further understanding of axial compression behavior can be gained by examining the buckled displacement patterns. If the Kirchhoff–Love kinematic hypothesis of classical theory is operative, then the axial and tangential displacements must be linear over the thickness and the radial displacement constant throughout. Plots of normalized displacements for a two-layer regular antisymmetric ($\pm 30^\circ$) laminate for $H/a = 0.01$ are shown in Fig. 6. The patterns for $L/a = 5$ and 100 abide by the Kirchhoff–Love hypothesis. But for $L/a = 0.2$, a short wavelength, the radial displacement pattern indicates the presence of transverse normal strain. Displacement plots for the same laminate profile for $H/a = 0.1$ are shown in Fig. 7. For this thick shell geometry, much greater transverse shear and normal strains can be observed for $L/a = 0.2$. Even for $L/a = 5$, the radial displacement wavers somewhat, suggesting the presence of some transverse normal deformation. The

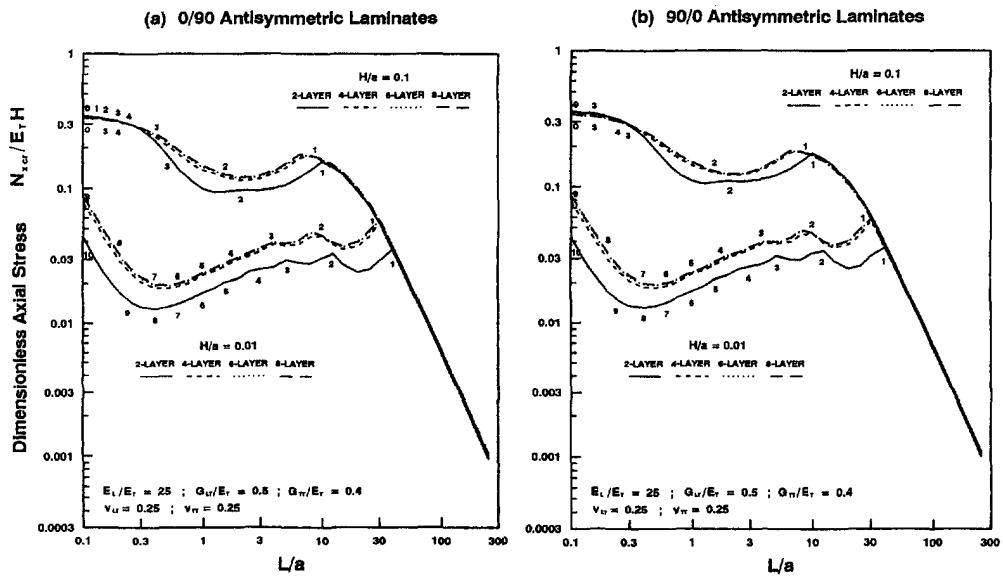

Fig. 3. Axial buckling of regular antisymmetric cross-ply cylinders.

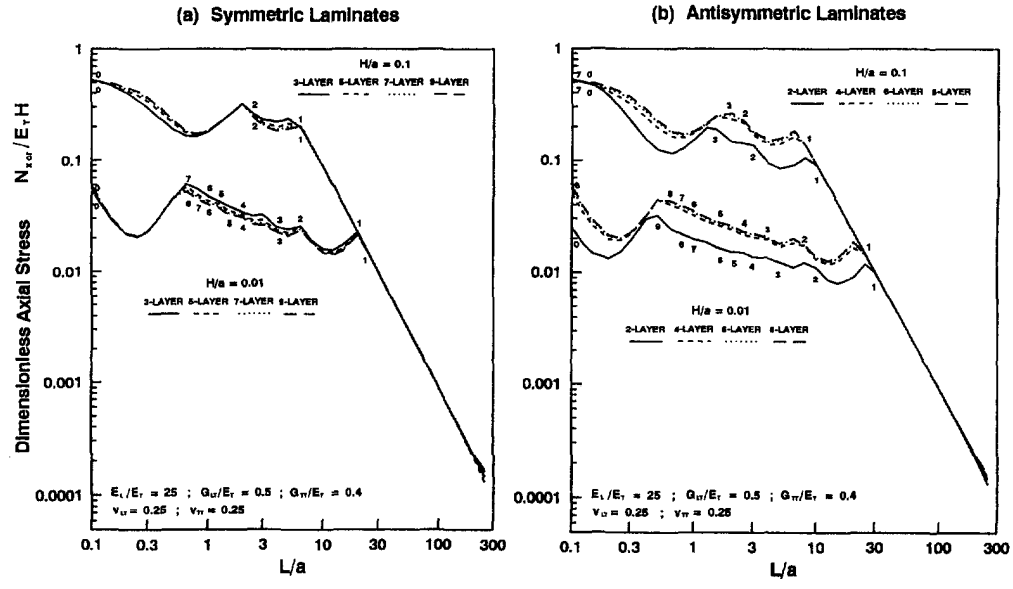

Fig. 4. Axial buckling of regular symmetric and antisymmetric ($\pm 45°$) cylinders.

accuracy of shell theory data is discussed in a companion paper by Etitum and Dong (1994).

Torsion

For torsion, the initial shear strain varies linearly from the central axis. Since the in-plane shear moduli of all ply materials are identical, all laminates are effectively homogeneous in torsion, so that the stress distribution is linear through the thickness in all cases. The lowest critical dimensionless shear stress is denoted by $N_{x\theta cr}/E_T H$, where $N_{x\theta}$ is the shear force per unit circumferential distance around the mid-surface of the cylinder. Plots of torsional stability data for the same laminate profiles that were considered in axial compression are shown in Figs 8–11.

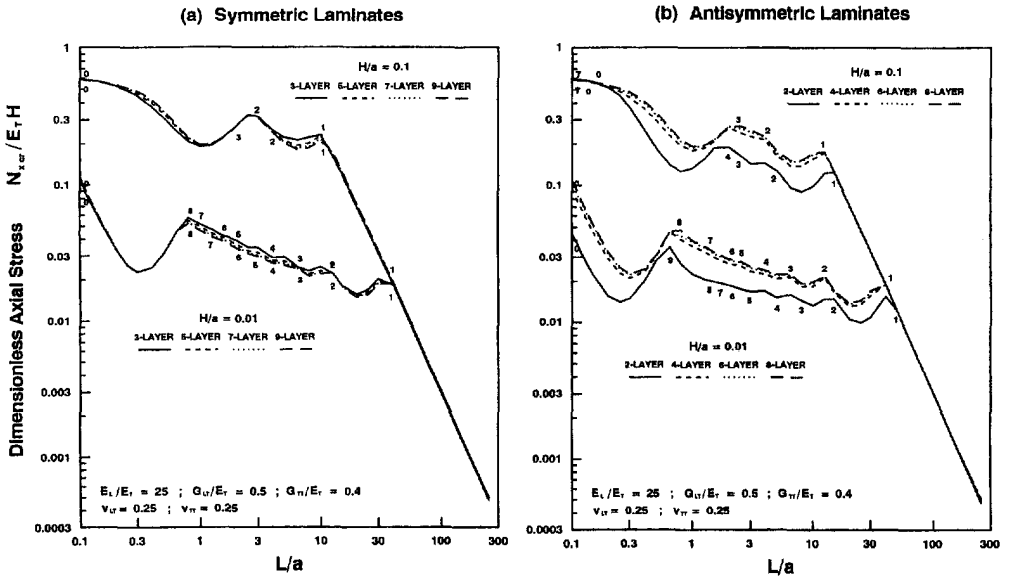

Fig. 5. Axial buckling of regular symmetric and antisymmetric ($\pm 30°$) cylinders.

By and large, trends similar to axial compression are evinced in torsional buckling. The direct correspondence of axial and shear stiffnesses to their buckling strengths can be seen by observing the difference between ($\pm 30°$) and ($\pm 45°$) laminates. For axial buckling, the ($\pm 30°$) laminates possessed higher critical stress as seen upon comparison of Figs 4 and 5, i.e. axial stiffness is higher in the ($\pm 30°$) than the ($\pm 45°$) orientation. For torsional stability, a greater buckling strength was evident in the ($\pm 45°$) laminates, i.e. maximum shear stiffness occurs at $\pm 45°$ orientations. No displacement plots are given for torsional buckling, as these data are not dramatically different from axial compression.

For large L/a, the circumferential mode number associated with the critical stress is $n = 1$. It is well known from studies based on shell theory that this mode is precluded if adjacent cross-sections between a given wavelength are restrained kinematically. The data herein are meaningful to the extent that the same periodic displacement field is employed in all cases.

THICK-WALLED CYLINDER

To illustrate the stability of a thick-walled cylinder, consider regular symmetric and antisymmetric ($\pm 30°$) laminated cylinders, all with thickness ratio of $H/a = 1$. The mechanical properties for the plies comprising these cylinders are those given by eqn (32). Again, the number of plies varied from three to nine for the symmetric profiles and two to eight for the antisymmetric profiles. The loading condition consisted of a uniform axial compressive strain over the entire cross-section.

Axial compression data are shown in Fig. 12, where the dimensionless axial stress $\sigma_{xx\,cr}/E_T$ is plotted against L/a for both symmetric and antisymmetric profiles. The data indicate that symmetric laminate profiles buckled at circumferential mode number $n = 0$ throughout the low to intermediate ranges of L/a, while antisymmetric laminate profiles buckled at high circumferential mode numbers. With an increasing L/a ratio, the circumferential mode number n decreased. For both cases in the range of L/a, large column instability is evident with $n = 1$. Also note that the buckling strengths of the two layer antisymmetric and three layer symmetric laminates in column instability regime are lower than those for laminate profiles of more plies. This behavior agrees with lamination theory, which shows that for a given laminate thickness, the flexural rigidity increases with the total number of plies.

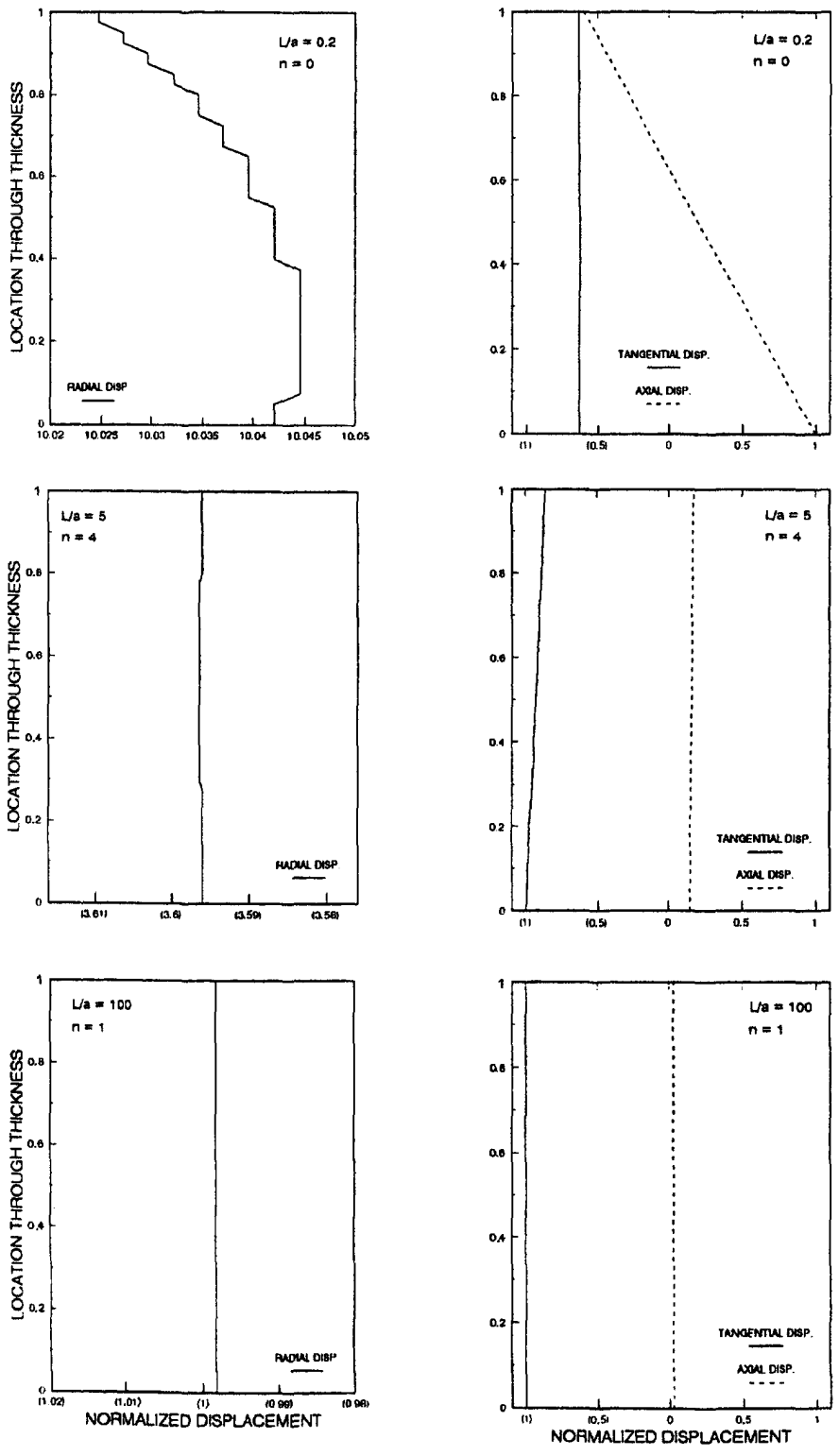

Fig. 6. Displacement patterns for regular antisymmetric two layer ($\pm 30°$) cylinder with $H/a = 0.01$.

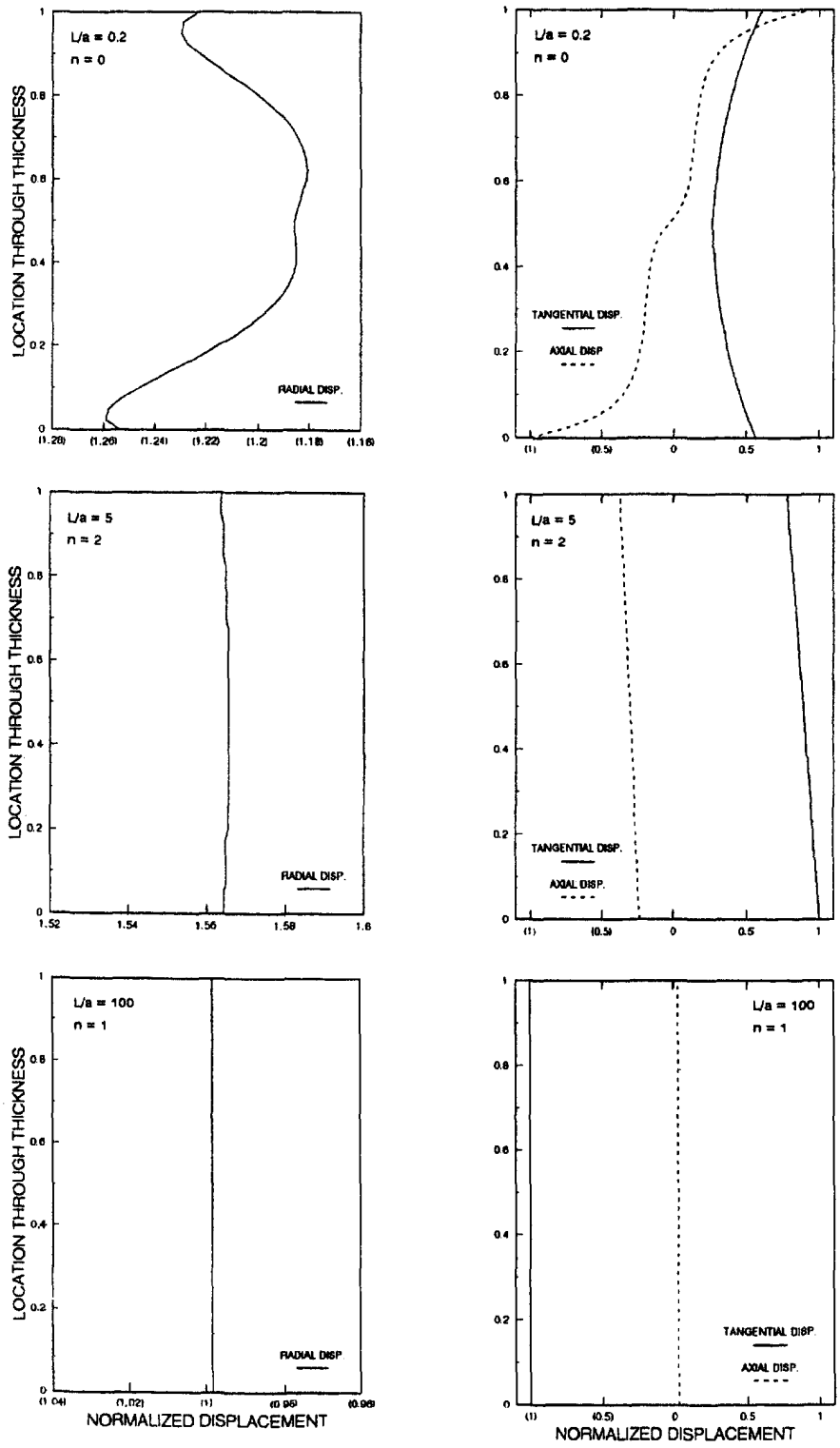

Fig. 7. Displacement patterns for regular antisymmetric two layer ($\pm 30°$) cylinder with $H/a = 0.1$.

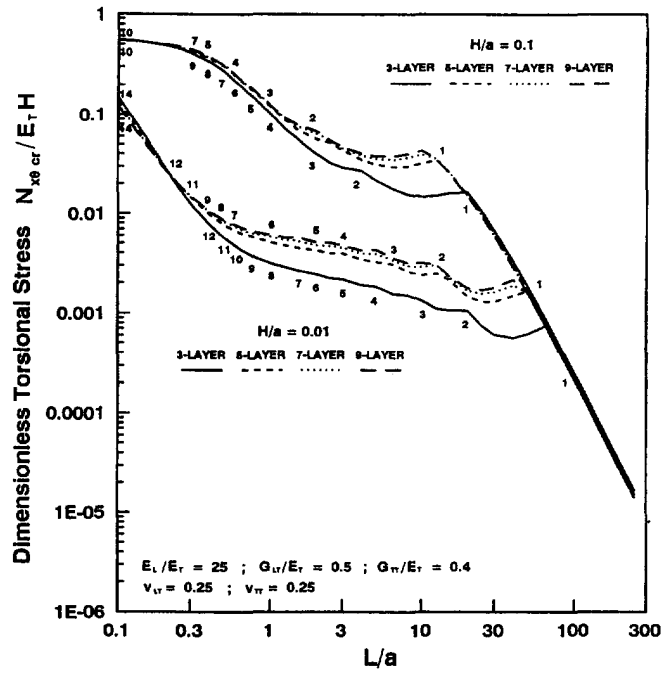

Fig. 8. Torsional buckling of regular symmetric cross-ply cylinders.

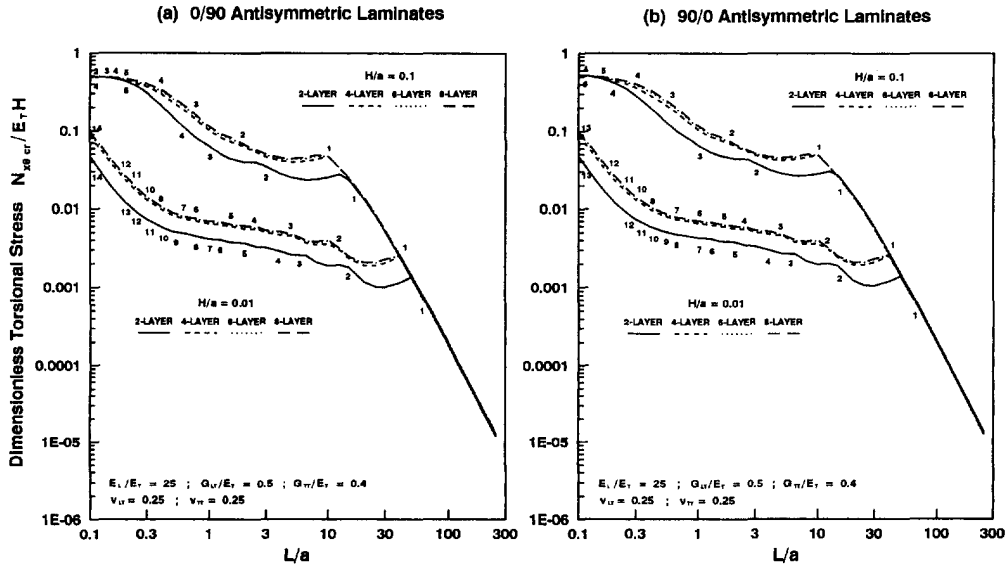

Fig. 9. Torsional buckling of regular antisymmetric cross-ply cylinders.

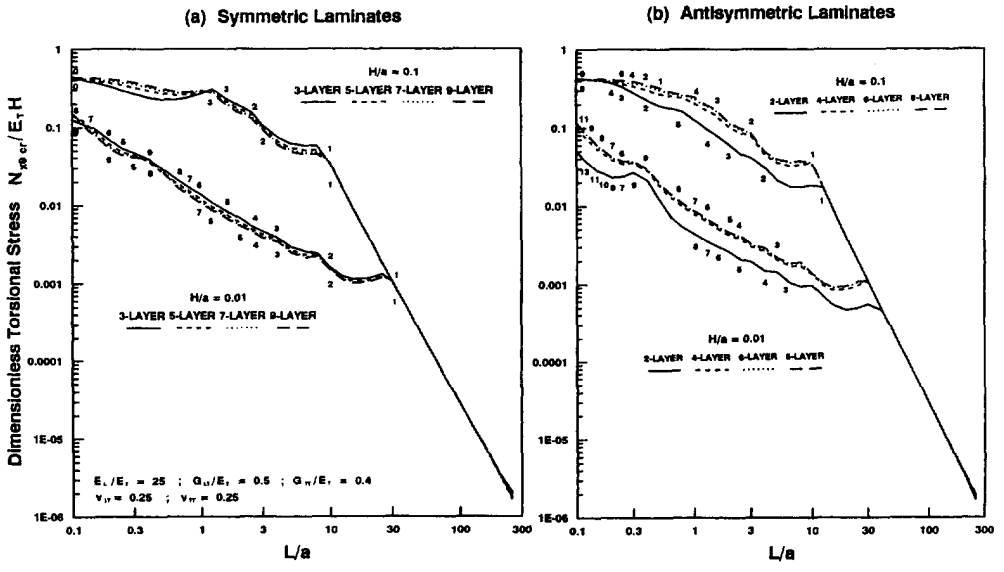

Fig. 10. Torsional buckling of regular symmetric and antisymmetric ($\pm 45°$) cylinders.

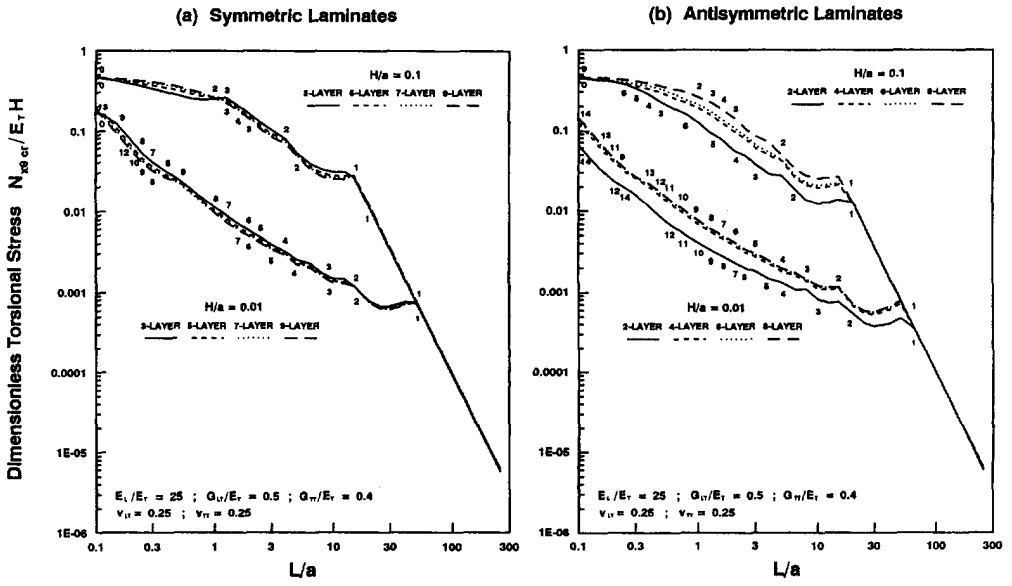

Fig. 11. Torsional buckling of regular symmetric and antisymmetric ($\pm 30°$) cylinders.

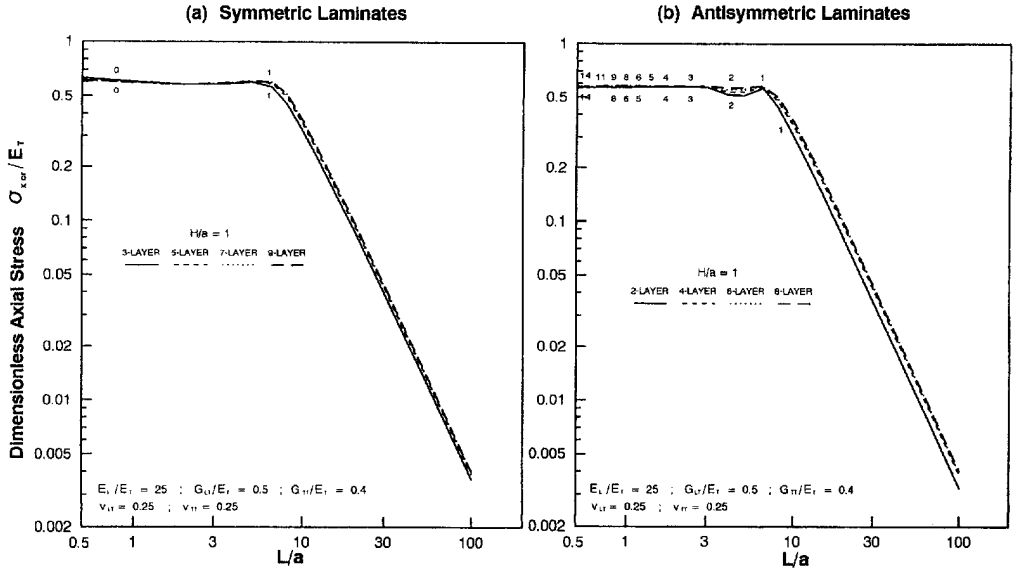

Fig. 12. Axial buckling of thick regular symmetric and antisymmetric ($\pm 30^\circ$) cylinders with $H/a = 1$.

Plots of displacement profiles over the laminate thickness for the three layer symmetric and two layer antisymmetric laminate profiles are shown in Figs 13 and 14, respectively. It can be seen that for both laminates, the behavior for $L/a = 100$ is that of column buckling, where the in-plane components are linear over the thickness and the radial component is constant throughout. The plots of the displacement fields for $L/a = 2$ and 0.5 show considerable transverse shear and normal deformations. Furthermore, for $L/a = 0.5$, the displacements are confined to a neighborhood near the outer surface, i.e. surface displacements where, with respect to a short buckling wave length, the total thickness resembles a half-space.

CONCLUDING REMARKS

A finite element method of analysis was presented for stability of circular cylindrical shells. The method is based on Biot's three-dimensional theory of incremental deformation. In this method, the discretization takes place in the thickness direction, where one-dimensional quadratic interpolations are used to represent the radial behavior of the three displacement components. For stability, an algebraic eigenvalue problem is generated, where the eigenvalues and eigenvectors represent the ratio of the critical stress state to the initial state and the corresponding displacement distribution over the thickness. Only the lowest (or critical) eigenvalue/eigenvector is of physical interest.

A parametric study of two geometries of cylindrical shells was carried out, i.e. $H/a = 0.01$ and 0.1 representing thin and thick shells, respectively. For these two thickness to radius ratios, number of plies, stacking sequence and fiber orientation were varied. From this study certain conclusions can be drawn regarding the ranges of validity of various shell theories, i.e. classical or refined.

An example of stability of a thick-walled cylinder was presented. The three-dimensional theory revealed that for long axial wavelengths, column stability behavior was in evidence. But for short axial wavelengths, the phenomenon involved surface instabilities, where the displacements occurred mainly in the region of the outer surface of the thick-walled cylinder. However, it should be remembered that for real materials, material yielding may occur before a full evolution of surface instability.

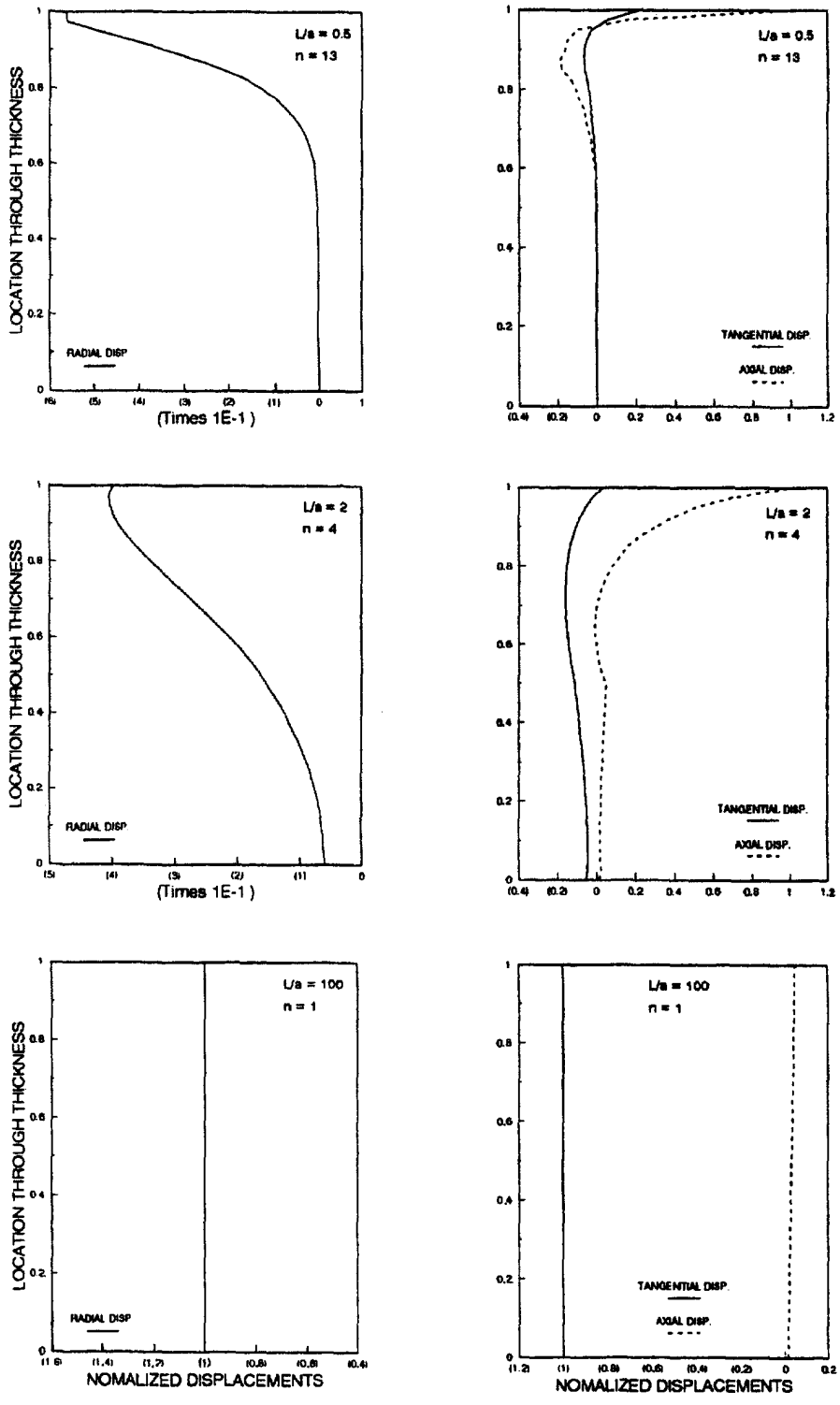

Fig. 13. Displacement patterns for regular antisymmetric two layer ($\pm 30°$) cylinder with $H/a = 1$.

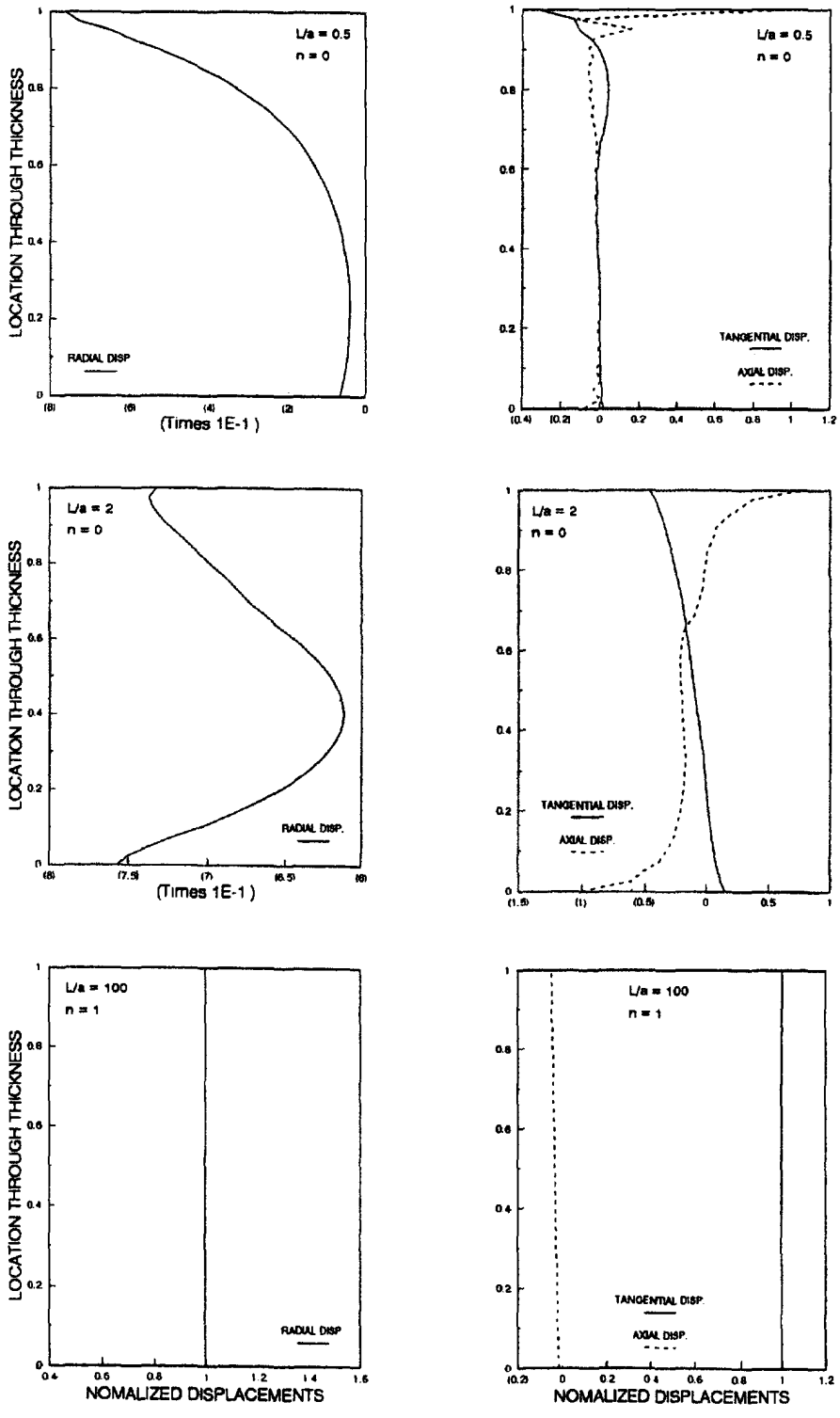

Fig. 14. Displacement patterns for regular symmetric three layer ($\pm 30°$) cylinder with $H/a = 1$.

REFERENCES

Biot, M. A. (1965). *Mechanics of Incremental Deformations*. Wiley and Sons, New York.

Bradford, L. G. and Dong, S. B. (1978). Natural vibrations of orthotropic cylinders under initial stress. *J. Sound Vibr.* **60**(2), 157–175.

Dong, S. B. and Wolf, J. A. (1970). Stability analysis of structures by a reduced system of generalized coordinates. *Int. J. Solids Structures* **6**, 1377–1388.

Dong, S. B., Wolf, J. A. and Peterson, F. E. (1972). On a direct-iterative eigensolution technique. *Int. J. Numer. Meth. Engng* **4**, 155–162.

Etitum, P. and Dong, S. B. (1994). A comparative study of stability of laminated anisotropic cylinders under axial compression and torsion. *Int. J. Solids Structures* **32**, 1231–1246.

Hutchinson, J. W. and Koiter, W. T. (1970). Postbuckling theory. *Appl. Mech. Rev.* **23**(12), 1353–1366.

Kantorovich, L. V. and Krylov, V. (1958). *Approximate Methods for Higher Analysis*. Noordhoff, Groningen, Netherlands.

Kardomateas, G. A. (1993a). Buckling of thick orthotropic cylindrical shells under external pressure. *J. Appl. Mech.* **60**(1), 195–202.

Kardomateas, G. A. (1993b). Stability loss in thick transversely isotropic cylindrical shells under axial compression. *J. Appl. Mech.* **60**(2), 506–513.

Pham, F. H. V. (1989). Analysis of initially stressed axisymmetric bodies by Biot's incremental theory. PhD Dissertation, University of California, Los Angeles.

Simitses, G. J. (1986). Buckling and postbuckling of imperfect cylindrical shells: a review. *Appl. Mech. Rev.* **39**(10), 1517–1524.

Tsai, S. W. and Hahn, T. (1980). *Introduction to Composite Materials*. Technomic, Westport, CT.

Zienkiewicz, O. C. (1978). *The Finite Element Method in Engineering Science*, 3rd Edition. McGraw-Hill, London.

APPENDIX

The operators in eqn (6) and strain–transformation matrices in eqns (16) and (17) are given by

$$L_{r1}=\begin{bmatrix} \partial/\partial r & \cdot & \cdot \\ 1/r & \cdot & \cdot \\ \cdot & \cdot & \cdot \\ \cdot & \cdot & \cdot \\ \cdot & \cdot & \partial/\partial r \\ \cdot & \partial/\partial r-1/r & \cdot \end{bmatrix},\quad \mathbf{B}_{r1}=\begin{bmatrix} N_r & \cdot & \cdot \\ N/r & \cdot & \cdot \\ \cdot & \cdot & \cdot \\ \cdot & \cdot & \cdot \\ \cdot & \cdot & N_r \\ \cdot & N_r-N/r & \cdot \end{bmatrix} \tag{A1a,g}$$

$$L_{\theta 1}=\frac{1}{r}\begin{bmatrix} \cdot & \cdot & \cdot \\ \cdot & \partial/\partial\theta & \cdot \\ \cdot & \cdot & \cdot \\ \cdot & \cdot & \partial/\partial\theta \\ \cdot & \cdot & \cdot \\ \partial/\partial\theta & \cdot & \cdot \end{bmatrix},\quad \mathbf{B}_{\theta 1}=\frac{1}{r}\begin{bmatrix} \cdot & \cdot & \cdot \\ \cdot & N & \cdot \\ \cdot & \cdot & \cdot \\ \cdot & \cdot & N \\ \cdot & \cdot & \cdot \\ N & \cdot & \cdot \end{bmatrix} \tag{A1b,h}$$

$$L_{x1}=\begin{bmatrix} \cdot & \cdot & \cdot \\ \cdot & \cdot & \cdot \\ \cdot & \cdot & \partial/\partial x \\ \cdot & \partial/\partial x & \cdot \\ \partial/\partial x & \cdot & \cdot \\ \cdot & \cdot & \cdot \end{bmatrix},\quad \mathbf{B}_{x1}=\begin{bmatrix} \cdot & \cdot & \cdot \\ \cdot & \cdot & \cdot \\ \cdot & \cdot & N \\ \cdot & N & \cdot \\ N & \cdot & \cdot \\ \cdot & \cdot & \cdot \end{bmatrix} \tag{A1c,i}$$

$$L_{r2}=\begin{bmatrix} \partial/\partial r & \cdot & \cdot \\ 1/r & \cdot & \cdot \\ \cdot & \cdot & \cdot \\ \cdot & \cdot & \cdot \\ \cdot & \cdot & \partial/2\,\partial r \\ \cdot & \partial/2\,\partial r-1/2r & \cdot \\ \cdot & \cdot & \cdot \\ \cdot & \cdot & \partial/2\,\partial r \\ \cdot & -\partial/2\,\partial r-1/2r & \cdot \end{bmatrix},\quad \mathbf{B}_{r2}=\frac{1}{2}\begin{bmatrix} 2N_r & \cdot & \cdot \\ 2N/r & \cdot & \cdot \\ \cdot & \cdot & \cdot \\ \cdot & \cdot & \cdot \\ \cdot & \cdot & N_r \\ \cdot & N_r-N/r & \cdot \\ \cdot & \cdot & \cdot \\ \cdot & \cdot & -N_r \\ \cdot & -N_r-N/r & \cdot \end{bmatrix} \tag{A1d,j}$$

$$L_{\theta 2}=\frac{1}{r}\begin{bmatrix} \cdot & \cdot & \cdot \\ \cdot & \partial/\partial\theta & \cdot \\ \cdot & \cdot & \cdot \\ \cdot & \cdot & \partial/2\,\partial\theta \\ \cdot & \cdot & \cdot \\ \partial/2\,\partial\theta & \cdot & \cdot \\ \cdot & \cdot & -\partial/2\,\partial\theta \\ \cdot & \cdot & \cdot \\ \partial/2\,\partial\theta & \cdot & \cdot \end{bmatrix} \quad \mathbf{B}_{\theta 2}=\frac{1}{2r}\begin{bmatrix} \cdot & \cdot & \cdot \\ \cdot & 2N & \cdot \\ \cdot & \cdot & \cdot \\ \cdot & \cdot & N \\ \cdot & \cdot & \cdot \\ N & \cdot & \cdot \\ \cdot & \cdot & -N \\ \cdot & \cdot & \cdot \\ N & \cdot & \cdot \end{bmatrix} \tag{A1e,k}$$

$$L_{x2}=\begin{bmatrix} \cdot & \cdot & \cdot \\ \cdot & \cdot & \cdot \\ \cdot & \cdot & \partial/\partial x \\ \cdot & \partial/2\,\partial x & \cdot \\ \partial/2\,\partial x & \cdot & \cdot \\ \cdot & \cdot & \cdot \\ \cdot & \partial/2\,\partial x & \cdot \\ -\partial/2\,\partial x & \cdot & \cdot \\ \cdot & \cdot & \cdot \end{bmatrix} \quad \mathbf{B}_{x2}=\frac{1}{2}\begin{bmatrix} \cdot & \cdot & \cdot \\ \cdot & \cdot & \cdot \\ \cdot & \cdot & 2N \\ \cdot & N & \cdot \\ N & \cdot & \cdot \\ \cdot & \cdot & \cdot \\ \cdot & N & \cdot \\ -N & \cdot & \cdot \\ \cdot & \cdot & \cdot \end{bmatrix}. \tag{A1f,l}$$